

Topological Anderson insulators with different bulk states in quasiperiodic chains

Ling-Zhi Tang,¹ Shu-Na Liu,¹ Guo-Qing Zhang,^{1,2} and Dan-Wei Zhang^{1,2,*}

¹Guangdong Provincial Key Laboratory of Quantum Engineering and Quantum Materials,
School of Physics and Telecommunication Engineering,

South China Normal University, Guangzhou 510006, China

²Guangdong-Hong Kong Joint Laboratory of Quantum Matter,
Frontier Research Institute for Physics, South China Normal University, Guangzhou 510006, China

(Dated: April 4, 2025)

We investigate the topology and localization of the one-dimensional Hermitian and non-Hermitian Su-Schrieffer-Heeger chains with quasiperiodic hopping modulations. In the Hermitian case, phase diagrams are obtained by numerically and analytically calculating various topological and localization characters. We show the presence of topological extended, intermediate, and localized phases due to the coexistence of topological and localization phase transitions. In particular, we uncover three types of disorder-induced topological Anderson insulators (TAIs) with extended, intermediate, and localized bulk states in this chiral chain. Moreover, we study the non-Hermitian effects on the TAIs by considering two kinds of non-Hermiticities from the non-conjugate hopping phase and asymmetric hopping strength, respectively. We demonstrate that three types of TAIs can preserve under the non-Hermitian perturbations with some unique localization and topological properties, such as the non-Hermitian real-complex and localization transitions and their topological nature.

I. INTRODUCTION

Topological insulators, hosting topological invariants for bulk states and nontrivial in-gap edge modes, have been widely explored in condensed matter [1, 2] and artificial systems [3–13]. Due to the global topology of band structures, topological insulators are immune to weak disorder or local perturbations. However, strong disorders usually drive the systems into trivial gapless insulators as all the bulk states becomes Anderson localized [14]. Unexpectedly, it was theoretically found that a topological phase transition from trivial phases to topological insulators with robust edge states can be driven by moderate disorders [15]. Such a disorder-induced topological phase is dubbed as topological Anderson insulators (TAI). Actually, the underlying mechanism of TAIs is the renormalization of topological terms by disorders [15–17], instead of the disorder-induced localization phenomenon.

In recent years, the TAIs and their generalizations have been revealed in various systems [15–29], even in some non-Hermitian systems [30–36] and in the presence of inter-particle interactions [37–39]. Some of them were experimentally observed in several engineered lattices, such as cold atomic gases [40], photonic and sonic crystals [41–43], electric circuits [44], and photonic quantum walks [35]. However, the interplay between disorder-induced topological and localization transitions remains largely unexplored. In particular, in most of these work, random disorders are considered and thus bulk states of the TAIs are fully localized, such as in one-dimensional (1D) Su-Schrieffer-Heeger (SSH) model [45] with random hopping strengths [19, 20, 40].

Quasiperiodic systems with incommensurate modulations in the potential or hopping terms are another platform to study the Anderson localization and topological phases of matter [46–65]. The quasiperiodic disorder can lead to unique localization phenomena without counterparts of random disorder in low dimensions, such as the localization transition [46–49], the intermediate phase consisting of both localized and extended states [50, 66–71], and the critical phase consisting of only critically localized states [64, 72–76]. Meanwhile, the topological charge pumping [48] can be realized in the paradigmatic 1D quasiperiodic Aubry-André-Harper model [46, 47] and its variety of generalizations [52–56, 59, 77, 78]. Very recently, the topological phase with critically localized bulk states in a quasiperiodic lattice [64] and the (non-quantized) pumping induced by the quasiperiodic disorder [65] were experimentally observed with cold atoms. However, it remains unclear whether the quasiperiodic disorder can induce TAIs with different localization properties of bulk states.

On the other hand, growing effort has recently been made to explore topological and localization physics in non-Hermitian Hamiltonians or systems [79–88]. For instance, in the presence of non-Hermiticities induced by non-reciprocal hopping [60, 89–92] or complex on-site potential [66, 91–95], it has been revealed that topological phase transition characterized by a spectral winding number coincides with localization transition and (or) real-complex transition [33, 60, 66, 95]. The non-Hermitian quasiperiodic systems may exhibit generalized mobility edge [91, 94]. Moreover, exotic non-Hermitian TAIs induced by non-reciprocal hopping terms with random disorders in the generalized SSH model has been proposed and observed in Refs. [30–35]. It would be interesting to further study the disorder-induced TAIs in non-Hermitian quasiperiodic systems.

In this work, we explore the interplay of topology and

* danweizhang@m.scnu.edu.cn

localization in the Hermitian and non-Hermitian SSH chains with quasiperiodic hopping disorders. In the Hermitian case, we obtain the phase diagrams by numerically calculating various topological and localization properties. The numerical results consist with the analysis of topological boundaries obtained from the localization length of zero modes and the self-consistent Born approximation (SCBA). We show the topological extended, intermediate (partially localized), and localized phases due to the coexistence of topological and localization phase transitions. In particular, we uncover three types of disorder-induced TAIIs with extended, intermediate, and localized bulk states in this system. Moreover, we study the non-Hermitian effects on the TAIIs by considering two kinds of non-Hermiticities from the non-conjugate complex hopping phase and asymmetric hopping strength, respectively. We find that the proposed three types of TAIIs can preserve under these non-Hermitian perturbations. We also reveal some unique localization and topological properties in these two cases, such as the non-Hermitian real-complex and localization transitions and their topological nature.

The rest of the paper are organized as follow. We first reveal three types of TAIIs in a Hermitian SSH chain with the quasiperiodic hopping modulation in Sec. II. Section III is then devoted to investigate non-Hermitian effects on the topological and localization properties of the uncovered TAIIs. A brief conclusion is presented in Sec. IV.

II. TAIIS WITH DIFFERENT BULK STATES

We start by considering a generalized SSH model in 1D dimerized lattice (denoted by A and B) with quasiperiodic disordered hopping, which is described by the following tight-binding Hamiltonian

$$H = \sum_{n=1}^N (m_n a_n^\dagger b_n + t a_{n+1}^\dagger b_n + \text{H.c.}), \quad (1)$$

where N is the number of unit cell, a_n^\dagger (b_n) denotes the creation (annihilation) operator for a particle on the A (B) sublattice of the n -th cell, and t and m_n is the constant inter-cell hopping strength and the site-dependent intra-cell hopping strength, respectively. In this Hermitian case ($H = H^\dagger$), we consider the quasiperiodic modulation on the intra-cell hopping term as

$$m_n = m + W \cos(2\pi\alpha n), \quad (2)$$

where m is an overall intra-cell hopping strength, W denotes the quasiperiodic disorder, and α is chosen as an irrational number to ensure the incommensurate modulation. In the clean limit with $W = 0$, the Hamiltonian in Eq. (1) reduces to the original SSH model with topological (trivial) phase when $m < t$ ($m > t$), which is characterized by the 1D winding number and protected by the chiral symmetry.

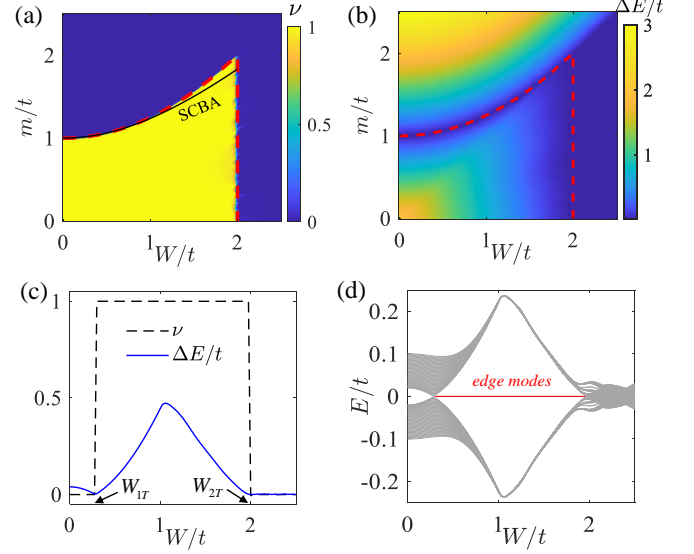


FIG. 1. (Color online) (a) Real-space winding number ν , (b) energy gap ΔE as functions of W and m . The red dash and black solid lines denote the topological phase boundaries determined by the divergence of the localization length of zero-energy states and from the SCBA analysis, respectively. (c) Plot of ν (red dash line) and ΔE (blue solid line) as a function of W for $m = 1.02$ with W_{1T} and W_{2T} being the topological transition points. (d) The middle 100 eigenenergies as a function of W for $m = 1.02$ under OBC, with two zero-energy edge modes when $W_{1T} < W < W_{2T}$ colored in red.

In the following, we investigate the quasiperiodic hopping disorder on the topology and localization in the model, which still preserves the chiral symmetry. We set $t = 1$ as the energy unit, $\alpha = (\sqrt{5} - 1)/2$ as the golden ratio, and the lattice size $N = 610$ in our numerical simulations. The periodic boundary condition (PBC) is considered unless mentioned otherwise.

A. Topological phase diagram and transitions

To characterize the topological properties of the disordered chiral chains that breaks the translation symmetry, one can use the real-space winding number defined by [20]

$$\nu = \frac{1}{L'} \text{Tr}'(\Gamma Q[Q, X]), \quad (3)$$

where $Q = \sum_{j=1}^N (|j\rangle\langle j|) - |\tilde{j}\rangle\langle\tilde{j}|$ denotes the flat-band Hamiltonian and is obtained by solving the equation $H|j\rangle = E_j|j\rangle$ and $|\tilde{j}\rangle = \Gamma^{-1}|j\rangle$ with eigenenergies E_j and eigenstates $|j\rangle$, $\Gamma = I_N \otimes \sigma_z$ is the chiral symmetry operator with the identity matrix I_N and the Pauli matrix σ_z , X is the coordinate operator, and Tr' denotes the trace over the middle interval of the lattice with the length $L' = L/2$.

The topological phase diagram on the W - m plane obtained by numerically computing ν is shown in Fig. 1(a).

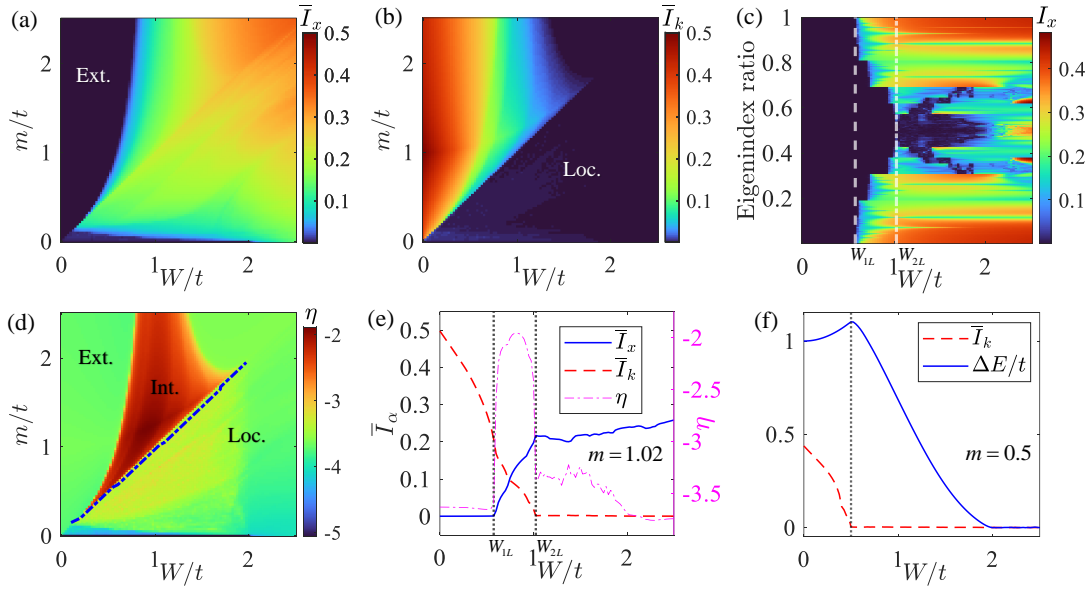


FIG. 2. (Color online) Averaged IPRs \bar{I}_x (a) and \bar{I}_k (b) and quantity η (d) on the parameter space $W-m$. (c) The IPR \bar{I}_x associated to eigenstates as a function of W for fixed $m = 1.02$. (e) Plots of \bar{I}_x (blue solid line), \bar{I}_k (red dash line) and η (pink dash-dot line) as a function of W with fixed $m = 1.02$. (f) Plot of \bar{I}_k (red dash line) and bulk gap ΔE (blue solid line) as a function of W for fixed $m = 0.5$. In (a,b,d), the regions for extended, localized and intermediate phases are denoted by 'Ext.', 'Loc.' and 'Int.', respectively. In (c,e), the vertical lines with $W_{1L} \approx 0.57$ and $W_{2L} \approx 1.02$ denote the first and second localization transitions, respectively. The blue dash-dot line in (d) denotes inflection point of ΔE with varying W .

In the clean limit $W = 0$, the topological transition between the trivial phase with $\nu = 0$ and the topological phase with $\nu = 1$ occurs at $m = 1$. The topological region for the constant intra-cell hopping strength m enlarges when increasing W to a modest regime. Thus one can find the TAI is driven by the quasiperiodic disorder from the trivial phase when $1 < m \lesssim 2$. This disorder-induced TAI is similar to that in the SSH model with random hopping disorders [19, 20, 40]. We also compute the bulk gap $\Delta E = E_{N+1} - E_N$ under the PBC, as shown in Fig. 1(b). The bulk gap closes at the topological transition points and becomes vanishing for trivial gapless Anderson insulators when W is large enough ($W \gtrsim 2$). To be more clear, we plot the ν and ΔE as a function of W for fixed $m = 1.02$ in Fig. 1(c). One can find the disorder-induced TAI lying between the first and second topological transition points at $W_{1T} \approx 0.27$ and $W_{2T} \approx 2.0$, respectively. The disorder-induced zero-energy edge modes in the energy spectrum of the TAI phase under the open boundary condition (OBC) are shown in Fig. 1(d), due to the bulk-boundary correspondence.

At the topological transition points, the localization length of zero-energy modes are divergent due to their delocalization nature in the chiral chains [20]. For our model Hamiltonian, the wave function of zero-energy eigenstate $\psi = \{\psi_{1,A}, \psi_{1,B}, \psi_{2,A}, \psi_{2,B} \dots \psi_{N,A}, \psi_{N,B}\}^T$ can be obtained by solving the corresponding Schrodinger equation $H\psi = 0$. This equation leads to $t\psi_{n,B} + m_n\psi_{n+1,B} = 0$ and $m_n\psi_{n,A} + t\psi_{n+1,A} = 0$, which leads to the form of the probability distribution

of the zero-energy wave function

$$\begin{aligned} \psi_{n,A} &= (-1)^n \prod_{l=1}^n \frac{m_l}{t} \psi_{1,A}, \\ \psi_{n,B} &= (-1)^n \prod_{l=1}^n \frac{t}{m_{l+1}} \psi_{1,B}. \end{aligned} \quad (4)$$

Thus, the inverse of localization length (Λ) of zero-energy modes in the limit $N \rightarrow \infty$ reads

$$\Lambda^{-1} = \max \left\{ \lim_{N \rightarrow \infty} \frac{1}{N} \ln |\psi_{N,A}|, \lim_{N \rightarrow \infty} \frac{1}{N} \ln |\psi_{N,B}| \right\}. \quad (5)$$

By setting $\psi_{1,A} = \psi_{1,B} = 1$, one can obtain

$$\begin{aligned} \lim_{N \rightarrow \infty} \frac{1}{N} \ln |\psi_{N,A}| &= \lim_{N \rightarrow \infty} \frac{1}{N} \ln |\psi_{N,B}| \\ &= \left| \lim_{N \rightarrow \infty} \frac{1}{N} \sum_{n=1}^N (\ln |t| - \ln |m_n|) \right|. \end{aligned} \quad (6)$$

Substituting Eq. (5) into Eq. (6), we obtain the inverse of the localization length of zero-energy modes as

$$\Lambda^{-1} = \left| \lim_{N \rightarrow \infty} \frac{1}{N} \sum_{l=1}^N (\ln |t| - \ln |m_l|) \right|. \quad (7)$$

Note that $\Lambda^{-1} \rightarrow 0$ when the localization length diverges ($\Lambda \rightarrow \infty$). We show the results of $\Lambda^{-1} \approx 0$ [numerically obtained by solving Eq. (7)] as the red dash lines in Figs.

1(a) and 1(b). The results indicate that topological and trivial phases can be well separated by the delocalization nature of zero modes in this quasiperiodic system, similar as those in random systems [20].

We further perform the SCBA analysis to reveal the disorder-induced renormalization of the topological term for the TAI in the topological phase diagram [Fig. 1(a)]. This analysis works in the region $W \lesssim 2$ where the disorder is not dominated. Based on the effective medium theory and the SCBA method [16], one can self-consistently obtain the disorder-induced self-energy as a renormalization in a clean Hamiltonian. For the Hamiltonian in Eq. (1), the self-energy term $\Sigma(W)$ satisfies the self-consistent equation

$$\frac{1}{E_F - H_q(k) - \Sigma(W)} = \left\langle \frac{1}{E_F - H_{\text{eff}}(k, W)} \right\rangle, \quad (8)$$

where $E_F \equiv 0$ is Fermi energy, $H_q(k) = [m + t \cos(k)]\sigma_x + t \sin(k)\sigma_y$ is the clean Hamiltonian ($W = 0$) in momentum space with $\sigma_{x,y}$ the Pauli matrices, $\Sigma = \Sigma_x\sigma_x + \Sigma_y\sigma_y$ and the $\langle \dots \rangle$ denotes averaging over all disorder samples. In our model, the disorder follow the form $V(n)\sigma_x$, thus the effective Hamiltonian H_{eff} is $H_{\text{eff}} = H_q(k) + V(n)\sigma_x$, where $V(n) = W \cos(2\pi\alpha n)$. Considering the symmetry of the Hamiltonian, the self-energy is simplified to a form $\Sigma(W) = \Sigma_x(W)\sigma_x$. The intra-cell hopping strength m is thus renormalized as $\bar{m} = m + \Sigma_x(W)$, with the topological phase boundaries at $\bar{m} = t$. The numerical results of $\bar{m}/t = 1$ shown as the black solid line in Fig. 1(a) agree well with the topological phase boundary determined by the winding number.

B. Localization properties of bulk states

We now study the localization properties in this model with the quasiperiodic hopping disorder. To reveal the localization of the bulk states, we can numerically compute the IPRs of the j -th eigenstate in real and momentum spaces

$$I_\beta(j) = \sum_\beta |\langle \beta | j \rangle|^4, \quad (9)$$

where the wave function $|j\rangle$ is normalized to unity and $\beta = x, k$ denotes the basis in real and momentum spaces, respectively. Here the momentum spaces wave function can be obtained by applying discrete Fourier transformation to the real space wave function [96]. For the large lattice size $L = 2N$ in our model, $I_x \sim \mathcal{O}(1)$ and $I_k \sim \mathcal{O}(L^{-1})$ indicate a localized eigenstate, while $I_x \sim \mathcal{O}(L^{-1})$ and $I_k \sim \mathcal{O}(1)$ for an extended eigenstate. The localization of the overall bulk states can be characterized by the averaged IPRs over the whole energy spectrum

$$\bar{I}_\beta = \frac{1}{L} \sum_{j=1}^L I_\beta(j). \quad (10)$$

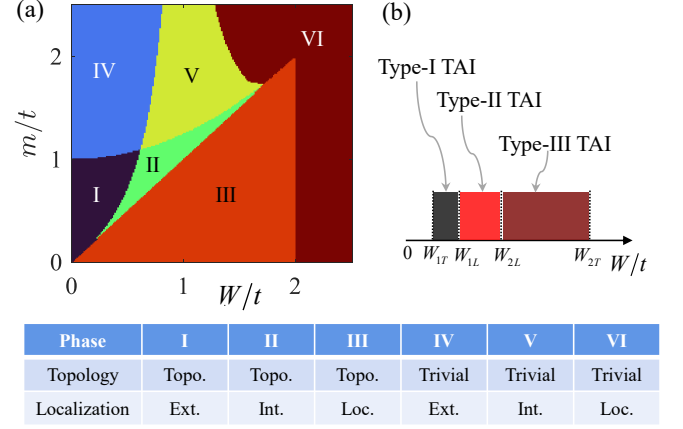


FIG. 3. (Color online) (a) Phase diagram on the W - m parameter space. There are six different phases: extended topological phase (I), topological intermediate phase (II), topological localized phase (III), trivial extended phase (IV), trivial intermediate phase (V), and trivial localized phase (VI), as illustrated in the table. (b) Regions of W with fixed $m = 1.02$ for three types of TAIs induced by the quasiperiodic disorder.

Figure 2(a) and 2(b) show the numerical results of \bar{I}_x and \bar{I}_k on the W - m plane, respectively. We can find the extended (localized) phase consisting of fully extended (localized) eigenstates with $\bar{I}_x \rightarrow 0$ ($\bar{I}_k \rightarrow 0$). However, there is an intermediate region with $\bar{I}_\beta \neq 0$ lying between the extended and localized phases on the W - m plane. To figure out the localization properties in this case, we display I_x as a function of W with respect to all eigenstates for $m = 1.02$ in Fig. 2(c). One can see that such an intermediate phase is partially localized (with the mobility edge) and consists of both extended and localized eigenstates lying between the first and second localization transition points at $W = W_{1L} \approx 0.57$ and $W = W_{2L} \approx 1.02$ [also see Fig. 2(e)], respectively.

To further characterize the intermediate phase, we can use the dimensional parameter

$$\eta = \log_{10}(\bar{I}_x \times \bar{I}_k). \quad (11)$$

Figure 2(d) displays the numerical results of η on the W - m plane, where the parameter region for the intermediate phase with relatively large η is clearly shown. We also plot $\bar{I}_{x,k}$ and η as a function of W with fixed $m = 1.02$ in Fig. 2(e). In the extended phase when $0 \leq W < W_{1L}$ and the localized phase when $W > W_{2L}$ with $W_{1L} \approx 0.57$ and $W_{2L} \approx 1.02$, one has vanishing \bar{I}_x and \bar{I}_k , respectively. In the intermediate phase when $W_{1L} < W < W_{2L}$, both of \bar{I}_x and \bar{I}_k are finite and thus takes a higher value of η . In addition, we numerically find that the inflection points of the energy gap ΔE with varying W nearly coincide with the transition points from the intermediate phase to the localized phase when $0.10 < W < 2.0$, which are denoted by the blue dash line in Fig. 2(d)). To see the coincidence, in Fig. 2(f), we plot ΔE and \bar{I}_k with varying W for $m = 0.5$ as an example.

Combining the topological and localization phase diagrams in Figs. 1(a) and 2(d), we finally obtain the phase diagram on the W - m plane, as shown in Fig. 3(a). There are totally six phases in the phase diagram determined by different topological and localization properties. They are labeled from I to VI: Phases I, II and III are topological with extended, intermediate, localized bulk states, respectively; and Phases IV, V and VI are trivial with extended, intermediate, localized bulk states, respectively. Thus, we obtain three types of TAIIs with different localization properties of bulk states. For instance, as shown in Fig. 3(b) with $m = 1.02$, one can find the disorder-driven transition from trivial extended phase to the TAIIs with extended ($W_{1T} < W < W_{1L}$), intermediate ($W_{1L} < W < W_{2L}$) and localized bulk states ($W_{2L} < W < W_{2T}$), which are dubbed as type-I, type-II and type-III TAIIs, respectively. For strong disorder ($W > W_{2T}$), the system becomes trivial gapless phase with fully localized states.

III. NON-HERMITIAN TAIIS

In this section, we proceed to study the non-Hermitian effects on the three types of TAIIs. In Sec. III A, we consider the non-Hermiticity induced by non-conjugate complex hopping phase. We also consider the asymmetric hopping strength in Sec. III B. We find that three types of TAIIs can preserve in these non-Hermitian cases without breaking the chiral symmetry, and can exhibit some properties unique to non-Hermitian systems.

A. Non-conjugate hopping-phase case

We now introduce the first non-Hermiticity to the hopping term of the model Hamiltonian in Eq. (1), which takes the following form

$$H' = \sum_{n=1}^N m'_n a_n^\dagger b_n + m'_n b_n^\dagger a_n + (t a_{n+1}^\dagger b_n + \text{H.c.}), \quad (12)$$

with the modified intra-cell hopping term

$$m'_n = m + W \cos(2\pi\alpha n + ih). \quad (13)$$

Here the non-Hermiticity can be controlled by the complex phase h [97], which leads to the non-conjugate hopping $m'_n \neq (m'_n)^*$ without breaking the chiral symmetry.

As shown in Refs. [30, 31, 98], the real-space winding number ν can be generalized to non-Hermitian Hamiltonians under the biorthogonal basis. To this end, the matrix Q in Eq. (3) is replaced by $Q = \sum_{j=1}^N (|j'R\rangle \langle j'L|) - |\tilde{j}'R\rangle \langle \tilde{j}'L|$ where right eigenstates $|j'R\rangle$ and left eigenstates $|j'L\rangle$ form the biorthogonal basis, obtained from the eigenfunctions $H' |j'R\rangle = E_{j'R} |j'R\rangle$ and $H^\dagger |j'L\rangle = E_{j'L} |j'L\rangle$ with $|j'R\rangle = \Gamma^{-1} |j'R\rangle$ and $|\tilde{j}'L\rangle = \Gamma^{-1} |j'L\rangle$. We numerically calculate ν on the W - m plane for

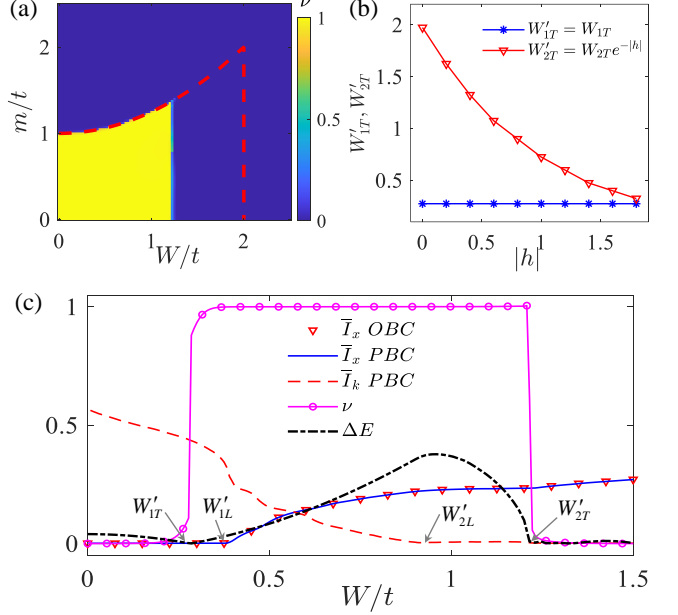


FIG. 4. (Color online) (a) ν as functions of W and m for $h = 0.5$. Red dash line denoted the topological phase boundary in the Hermitian case ($h = 0$). (b) The first and second topological transition points W'_{1T} and W'_{2T} for varying non-Hermiticity parameter $|h|$ and fixed $m = 1.02$. (c) ν , $\bar{I}_{x,k}$ (under the PBC and OBC), and ΔE as a function of W for $m = 1.02$ and $h = 0.5$. The two topological and localization transition points at $W'_{1T} \approx 0.27$, $W'_{2T} \approx 1.21$, $W'_{1L} \approx 0.39$, and $W'_{2L} \approx 0.92$ are labeled.

$h = 0.5$, as shown in Fig. 4(a), where the red dash line denotes the topological phase boundary in the Hermitian case [$h = 0$ in Fig. 1(a)]. One can find that this non-Hermiticity with finite $|h|$ reduces the topological region by moving the second topological transition from W_{2T} to $W'_{2T} < W_{2T}$, while keeps the first topological transition at $W'_{1T} = W_{1T} < W'_{2T}$. To see this point more clearly, we plot the W'_{1T} and W'_{2T} as a function $|h|$ for fixed $m = 1.02$ in Fig. 4(b), which are well fitting by $W'_{1T} = W_{1T}$ and $W'_{2T} = W_{2T}e^{-|h|}$, with $W_{1T} \approx 0.27$ and $W_{2T} \approx 2.0$ in the Hermitian limit.

In Fig. 4(c), we plot the winding number ν and the energy gap $\Delta E = \text{Re}(E_{N+1,R} - E_{N,R})$ defined by the real part of the complex eigenenergies $E_{N,R}$ (sorted by the real part of spectrum) as a function of W for $m = 1.02$ and $h = 0.5$. The two topological phase transitions happen at $W'_{1T} \approx 0.27$ and $W'_{2T} \approx 1.21$ with the gap closing. To reveal the localization properties in this non-Hermitian case, we calculate the IPRs \bar{I}_β averaged over the right eigenstates $|jR\rangle$. The results of \bar{I}_x are the same under PBC and OBC in both the clean and disordered cases. This indicates the absence of non-Hermitian skin effect [84–88] of bulk states under OBC. With the results of \bar{I}_β , we can obtain the first and second localization transition points at $W'_{1L} \approx 0.39$ and $W'_{2L} \approx 0.92$. Thus, the three types of TAIIs can still be induced by the quasiperiodic disorder in this non-Hermitian system

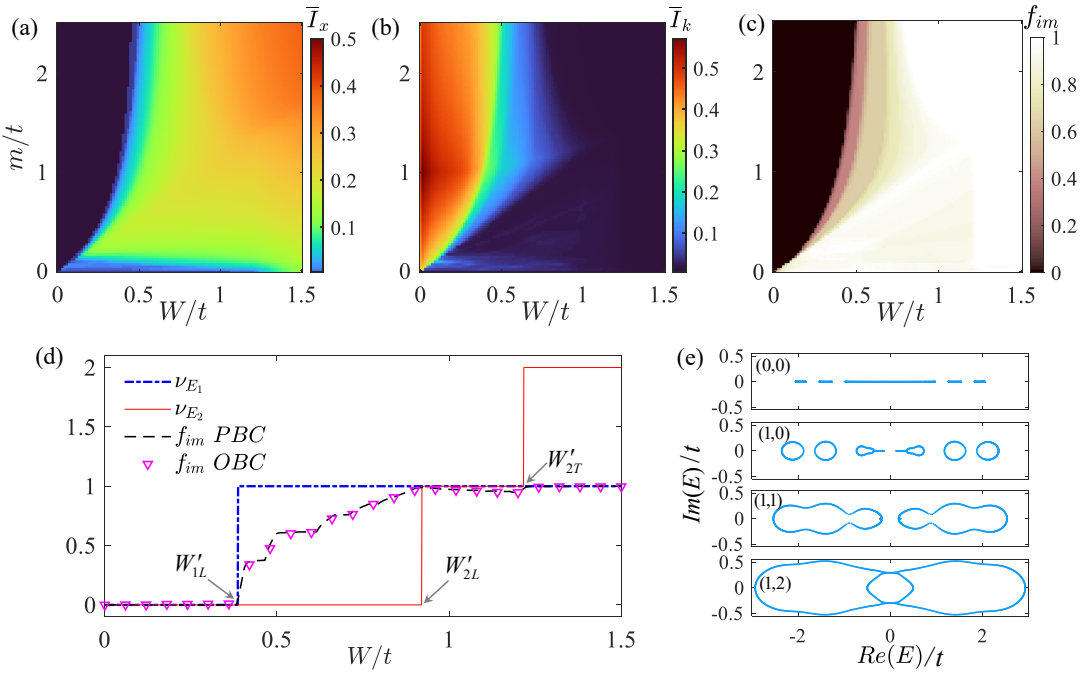


FIG. 5. (Color online) Averaged IPR \bar{I}_x (a) and \bar{I}_k (b) and ratio of complex eigenenergies f_{im} (c) under PBC for $h = 0.5$ on the parameter space $W-m$. (d) Plot of spectral winding number ν_{E_1} (blue dash line), ν_{E_2} (red dash line), f_{im} for PBC (black dash line) and f_{im} for OBC (pink inverted triangle) for $m = 1.02$, $h = 0.5$ as a function of W . The two localization transition points $W'_{1L} \approx 0.39$ and $W'_{2L} \approx 0.92$, and the topological transition point $W'_{2T} \approx 1.21$ are labeled. (e) Typical energy spectrum for $W = 0.3, 0.8, 1, 1.4$ (from top to bottom) with the energy winding numbers (ν_{E_1}, ν_{E_2}) in each panel for $h = 0.5$.

when $0.27 \lesssim W \lesssim 0.39$ (type-I), $0.39 \lesssim W \lesssim 0.92$ (type-II), and $0.92 \lesssim W \lesssim 1.21$ (type-III), respectively. In Figs. 5(a) and 5(b), we further show the results of $\bar{I}_{x,k}$ under PBC on the $W-m$ plane with $h = 0.5$. Comparing to the results for $h = 0$ in Figs. 2(a) and 2(b), we can find that non-Hermiticity enlarges the parameter regions of the localized phase and reduces the extended and intermediate phase regions. The result indicates that the non-conjugate hopping tends to localize the bulk states.

The real-complex transition of the energy spectrum and its winding on the complex energy plane are unique to non-Hermitian Hamiltonians [79–81]. To study the real-complex transition in this non-Hermitian case with non-conjugate hopping phases, we numerically compute the ratio of the right eigenstates $|jR\rangle$ with complex eigenenergies in the energy spectrum, which is defined by

$$f_{im} = L_{im}/L, \quad (14)$$

with L_{im} the number of eigenenergies whose imaginary part $|\text{Im}(E_{jR})| > 10^{-13}$ as the cutoff in our simulations. The numerical result of f_{im} for $h = 0.5$ on the $W-m$ plane is shown in Fig. 5(c). We find that the energy spectrum is either real ($f_{im} = 0$) or complex ($0 < f_{im} \leq 1$) in the phase diagram. The boundary between the real and complex energies corresponds to the localization-delocalization phase boundary in Fig. 5(a). To see the coincidence more clearly, we plot f_{im} under PBC and

OBC as a function of W in Fig. 5(d), with the localization transition points W'_{1L} and W'_{2L} being labeled. One can see that that f_{im} turns to non-zero at W'_{1L} , which shows that the real-complex transition coincides with the localization transition from the extended to intermediate phases. In addition, $f_{im} \approx 1$ in the fully localized phase when $W \gtrsim W'_{2L}$. Here the independence of f_{im} on the boundary condition indicates the absence of the non-Hermitian skin effect in this non-conjugate hopping-phase case.

To characterize the topology of the energy spectrum in our non-Hermitian quasiperiodic chains, we can use the spectral winding numbers defined as [82]

$$\nu_\mu = \int_0^{2\pi} \frac{d\theta}{2\pi i} \partial_\theta \ln \det [\mathcal{H}(\theta) - \mu]. \quad (15)$$

Here the modified Hamiltonian $\mathcal{H}(\theta) = H'(\theta)$ with respect to the additional periodic modulation phase θ is given by rewriting m'_n in Eq. (12) as

$$m'_n(\theta) = m + W \cos(2\pi\alpha n + ih + \theta). \quad (16)$$

In addition, the indexes $\mu = E_1, E_2$ denote the real parts of eigenenergies for the eigenstates with the smallest and maximum IPRs I_x (for the most extended and localized eigenstates), respectively. Unlike the chiral winding number ν for eigenstates, here ν_μ counts how many times the complex eigenenergies trails enclosing the energy base μ on the complex plane when θ changes from 0 to 2π . Thus,

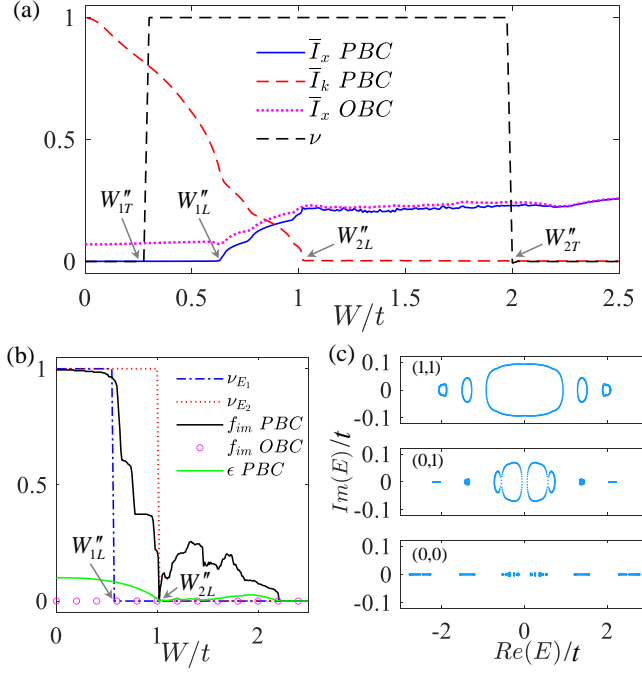


FIG. 6. (Color online) (a) Plots of $\bar{I}_{x,k}$ (under the PBC and OBC) and ν as a function of W . The two topological transition points at $W''_1 \approx 0.27$ and $W''_2 \approx 2.0$, and two localization transition points $W''_1 \approx 0.63$ and $W''_2 \approx 1.02$ are labeled. (b) ν_{E_1} (blue dash-dot line), ν_{E_2} (red dot line), f_{im} under PBC (black solid line), f_{im} under OBC (pink round), max imaginary part of energy spectrum ϵ (green solid line) as functions of W . (c) Energy spectrum for $W = 0.4, 0.7, 1.4$ (from top to bottom) with corresponding (ν_{E_1}, ν_{E_2}) inside each panel. The other parameters fixed $m = 1.02$ and $g = 0.1$.

ν_μ characterizes the topological structure of the complex spectrum, instead of the number of edge modes.

The numerical results of ν_μ for $h = 0.5$ as a function of W are shown in Fig. 5(d). We find that the values of ν_{E_1} and ν_{E_2} change at W'_1 and W'_2 , respectively. In this non-Hermitian chain, the extended and intermediate phases can be characterized by $(\nu_{E_1}, \nu_{E_2}) = (0,0)$ and $(1,0)$ respectively, while the localized phase takes $(\nu_{E_1}, \nu_{E_2}) = (1,1)$ or $(1,2)$. This correspondence can be understood in the assistance of the eigenenergies spectrum shown in Fig. 5(e), with the disorder strength $W = 0.3, 0.8, 1, 1.4$ (from the top to the bottom panel) for four typical cases. When $W < W'_1$ with $W = 0.3$, $\nu_{E_1} = \nu_{E_2} = 0$ due to the real spectrum with $f_{im} = 0$. When $W'_1 < W < W'_2$ with $W = 0.8$, part of eigenstates become localized with complex eigenenergies that encloses E_1 on the complex plane and thus leads to $\nu_{E_1} = 1$. When $W'_2 < W < W''_2$ with $W = 1$, most eigenenergies become complex with $f_{im} \approx 1$ and enclose $E_{1,2}$ with $\nu_{E_1} = \nu_{E_2} = 1$. Interestingly, we find that the transition from $\nu_{E_2} = 1$ to $\nu_{E_2} = 2$ coincides with that from $\nu = 1$ to $\nu = 0$ at W''_2 due to the band crossing at this topological transition point. These results indicate the coincidence of disorder-induced real-complex, local-

ization and topological transitions, as well as the existence of the three types of TAIs in this non-Hermitian quasiperiodic lattice.

B. Asymmetric hopping-strength case

We consider another kind of non-Hermiticity induced by the asymmetric hopping strength in our model, which reads

$$H'' = \sum_{n=1}^N (m_n a_n^\dagger b_n + \text{H.c.}) + t e^{-g} a_{n+1}^\dagger b_n + t e^{g} b_n^\dagger a_{n+1}. \quad (17)$$

Here g denotes the non-reciprocal parameter. Notably, in this case $\mathcal{H}(\theta) = H''(\theta)$ in Eq. (15), with $H''(\theta)$ defined by adding the periodically twisted phase θ to the asymmetric hopping under the PBC: $g \rightarrow g - i\theta/L$ in Eq. (17). We plot ν as a function of W for $m = 1.02$ and $g = 0.1$ in Fig. 6(a). The disorder-induced topological transitions in this case happen at $W = W''_1 = W_1 \approx 0.27$ (from trivial phase to TAIs) and $W = W''_2 = W_2 \approx 2.0$ (from TAIs to trivial phase). This can be understood from the fact that H'' can be transformed to H under OBC through a similarity transformation $H = SH''S^{-1}$ with $S = \text{diag}\{1, 1, e^{-g}, e^{-g}, e^{-2g}, e^{-2g}, \dots, e^{-Ng}, e^{-Ng}\}$. The corresponding eigenstates $|j''\rangle$ can be obtained via $|j''\rangle = S^{-1}|j\rangle$ with the same real eigenenergies of H . This leads to the non-Hermitian skin effect for bulk states of H'' under the OBC.

We also calculate $\bar{I}_{x,k}$ to study the localization properties. The localization transition points $W''_1 \approx 0.63 > W_1$ and $W''_2 = W_2 \approx 1.02$ with increasing g . Thus, the asymmetry hopping tends to enlarge (keep) the extend (fully localized) phase region and reduces the intermediate phase region. Notably, the real-space averaged IPRs \bar{I}_x under OBC is larger than that under PBC in extended and intermediate phase due to the non-Hermitian skin effect [30]. In the localized phase for $W > W''_2$, \bar{I}_x takes nearly the same values for OBCs and PBCs as the skin effect of bulk states is destroyed by strong disorders.

In Fig. 6(b), we numerically calculate ν_μ , the imaginary fraction f_{im} and the maximum value of the imaginary part in the energy spectrum $\epsilon = \max[\text{Im}(E_j)]$ as a function of W for $m = 1.02$ and $g = 0.1$. In this asymmetric hopping case, the eigenenergies of H'' under OBC shares the same real spectrum of H , such that $f_{im} = 0$ for all W and there is no real-complex transition under OBC. In addition, ν_{E_1} and ν_{E_2} change at the localization transition points W''_1 and W''_2 , respectively. However, the disorder-induced real-complex transition under PBC happens at $W \approx 2.21 > W''_2 > W''_1$. We also plot the energy spectra for $W = 0.3, 0.8, 1.4$ in Fig. 6(c). When $0 \leq W < W''_1$ with $W = 0.3$, complex eigenenergies encloses E_1 and E_2 with $f_{im} \approx 1$ and $\nu_{E_1} = \nu_{E_2} = 1$. Increasing disorder strength when $W''_1 < W < W''_2$ with $W = 0.8$, part of eigenenergies become real and thus $\nu_{E_2} = 0$. When $W > W''_2$ with $W = 1.4$, most eigenen-

ergies become real with $f_{im} \approx 0$ and $\epsilon \approx 0$, such that $\nu_{E_1} = \nu_{E_2} = 0$. These results indicate that the existence of the three types of TAIs in under the asymmetric hopping strengths. The disorder-induced localization transition coincides with the real-complex transition under PBC, but are not related to the topological transition in this non-Hermitian case.

IV. CONCLUSION

In summary, we have explored the topology and localization of Hermitian and non-Hermitian SSH chains with quasiperiodic hopping disorders. In the Hermitian case, we have obtained the phase diagrams with topological extended, intermediate and localized phases. Due to the coexistence of topological and localization transitions, we uncovered three types of disorder-induced TAIs with extended, intermediate, and localized bulk states in the system. We have also studied the non-Hermitian effects on

the TAIs by considering two kinds of non-Hermiticities from the non-conjugate hopping phase and asymmetric hopping strength, respectively. We have shown that the three types of TAIs can preserve and exhibit some unique localization and topological properties in these non-Hermitian systems.

ACKNOWLEDGMENTS

This work was supported by the National Natural Science Foundation of China (Grants No. 12174126 and No. 12104166), the Key-Area Research and Development Program of Guangdong Province (Grant No. 2019B030330001), the Science and Technology Program of Guangzhou (Grant No. 2019050001), and the Guangdong Basic and Applied Basic Research Foundation (Grants No. 2021A1515010315 and No. 2020A1515110290).

[1] X.-L. Qi and S.-C. Zhang, *Rev. Mod. Phys.* **83**, 1057 (2011).

[2] M. Z. Hasan and C. L. Kane, *Rev. Mod. Phys.* **82**, 3045 (2010).

[3] D.-W. Zhang, Y.-Q. Zhu, Y. X. Zhao, H. Yan, and S.-L. Zhu, *Advances in Physics* **67**, 253 (2018).

[4] N. R. Cooper, J. Dalibard, and I. B. Spielman, *Rev. Mod. Phys.* **91**, 015005 (2019).

[5] N. Goldman, J. C. Budich, and P. Zoller, *Nat. Phys.* **12**, 639 (2016).

[6] M. D. Schroer, M. H. Kolodrubetz, W. F. Kindel, M. Sandberg, J. Gao, M. R. Vissers, D. P. Pappas, A. Polkovnikov, and K. W. Lehnert, *Phys. Rev. Lett.* **113**, 050402 (2014).

[7] P. Roushan, C. Neill, Y. Chen, M. Kolodrubetz, C. Quintana, N. Leung, M. Fang, R. Barends, B. Campbell, Z. Chen, B. Chiaro, A. Dunsworth, E. Jeffrey, J. Kelly, A. Megrant, J. Mutus, P. J. J. O’Malley, D. Sank, A. Vainsencher, J. Wenner, T. White, A. Polkovnikov, A. N. Cleland, and J. M. Martinis, *Nature* **515**, 241 (2014).

[8] X. Tan, D.-W. Zhang, Q. Liu, G. Xue, H.-F. Yu, Y.-Q. Zhu, H. Yan, S.-L. Zhu, and Y. Yu, *Phys. Rev. Lett.* **120**, 130503 (2018).

[9] X. Tan, D.-W. Zhang, Z. Yang, J. Chu, Y.-Q. Zhu, D. Li, X. Yang, S. Song, Z. Han, Z. Li, Y. Dong, H.-F. Yu, H. Yan, S.-L. Zhu, and Y. Yu, *Phys. Rev. Lett.* **122**, 210401 (2019).

[10] C. H. Lee, S. Imhof, C. Berger, F. Bayer, J. Brehm, L. W. Molenkamp, T. Kiessling, and R. Thomale, *Communications Physics* **1**, 39 (2018).

[11] S. D. Huber, *Nature Physics* **12**, 621 (2016).

[12] L. Lu, J. D. Joannopoulos, and M. Soljačić, *Nature Photonics* **8**, 821 (2014).

[13] T. Ozawa, H. M. Price, A. Amo, N. Goldman, M. Hafezi, L. Lu, M. C. Rechtsman, D. Schuster, J. Simon, O. Zilbermanberg, and I. Carusotto, *Rev. Mod. Phys.* **91**, 015006 (2019).

[14] P. W. Anderson, *Phys. Rev.* **109**, 1492 (1958).

[15] J. Li, R.-L. Chu, J. K. Jain, and S.-Q. Shen, *Phys. Rev. Lett.* **102**, 136806 (2009).

[16] C. W. Groth, M. Wimmer, A. R. Akhmerov, J. Tworzydło, and C. W. J. Beenakker, *Phys. Rev. Lett.* **103**, 196805 (2009).

[17] H. Jiang, L. Wang, Q.-F. Sun, and X. C. Xie, *Phys. Rev. B* **80**, 165316 (2009).

[18] H.-M. Guo, G. Rosenberg, G. Refael, and M. Franz, *Phys. Rev. Lett.* **105**, 216601 (2010).

[19] A. Altland, D. Bagrets, L. Fritz, A. Kamenev, and H. Schmiedt, *Phys. Rev. Lett.* **112**, 206602 (2014).

[20] I. Mondragon-Shem, T. L. Hughes, J. Song, and E. Prodan, *Phys. Rev. Lett.* **113**, 046802 (2014).

[21] P. Titum, N. H. Lindner, M. C. Rechtsman, and G. Refael, *Phys. Rev. Lett.* **114**, 056801 (2015).

[22] B. Wu, J. Song, J. Zhou, and H. Jiang, *Chinese Physics B* **25**, 117311 (2016).

[23] P. V. Sriluckshmy, K. Saha, and R. Moessner, *Phys. Rev. B* **97**, 024204 (2018).

[24] J.-H. Zheng, T. Qin, and W. Hofstetter, *Phys. Rev. B* **99**, 125138 (2019).

[25] Y. Kuno, *Phys. Rev. B* **100**, 054108 (2019).

[26] R. Chen, D.-H. Xu, and B. Zhou, *Phys. Rev. B* **100**, 115311 (2019).

[27] X. S. Wang, A. Brataas, and R. E. Troncoso, *Phys. Rev. Lett.* **125**, 217202 (2020).

[28] C.-A. Li, B. Fu, Z.-A. Hu, J. Li, and S.-Q. Shen, *Phys. Rev. Lett.* **125**, 166801 (2020).

[29] Y.-B. Yang, K. Li, L.-M. Duan, and Y. Xu, *Phys. Rev. B* **103**, 085408 (2021).

[30] D.-W. Zhang, L.-Z. Tang, L.-J. Lang, H. Yan, and S.-L. Zhu, *Sci. China-Phys. Mech. Astron.* **63**, 267062 (2020).

[31] X.-W. Luo and C. Zhang, *arXiv:1912.10652v1*.

[32] H. Wu and J.-H. An, *Phys. Rev. B* **102**, 041119 (2020).

[33] L.-Z. Tang, L.-F. Zhang, G.-Q. Zhang, and D.-W. Zhang, *Phys. Rev. A* **101**, 063612 (2020).

[34] H. Liu, Z. Su, Z.-Q. Zhang, and H. Jiang, *Chinese Physics B* **29**, 050502 (2020).

[35] Q. Lin, T. Li, L. Xiao, K. Wang, W. Yi, and P. Xue, (2021), arXiv:2108.01097 [cond-mat.mes-hall].

[36] J. Claes and T. L. Hughes, *Phys. Rev. B* **103**, L140201 (2021).

[37] G.-Q. Zhang, L.-Z. Tang, L.-F. Zhang, D.-W. Zhang, and S.-L. Zhu, *Phys. Rev. B* **104**, L161118 (2021).

[38] K. Li, J.-H. Wang, Y.-B. Yang, and Y. Xu, arXiv (2021), arXiv:2104.14097 [cond-mat.dis-nn].

[39] T.-C. Yi, S. Hu, E. V. Castro, and R. Mondaini, *Phys. Rev. B* **104**, 195117 (2021).

[40] E. J. Meier, F. A. An, A. Dauphin, M. Maffei, P. Massignan, T. L. Hughes, and B. Gadway, *Science* **362**, 929 (2018).

[41] S. Stützer, Y. Plotnik, Y. Lumer, P. Titum, N. H. Lindner, M. Segev, M. C. Rechtsman, and A. Szameit, *Nature* **560**, 461 (2018).

[42] G.-G. Liu, Y. Yang, X. Ren, H. Xue, X. Lin, Y.-H. Hu, H.-x. Sun, B. Peng, P. Zhou, Y. Chong, and B. Zhang, *Phys. Rev. Lett.* **125**, 133603 (2020).

[43] F. Zangeneh-Nejad and R. Fleury, *Advanced Materials* **32**, 2001034 (2020).

[44] W. Zhang, D. Zou, Q. Pei, W. He, J. Bao, H. Sun, and X. Zhang, *Phys. Rev. Lett.* **126**, 146802 (2021).

[45] W. P. Su, J. R. Schrieffer, and A. J. Heeger, *Phys. Rev. Lett.* **42**, 1698 (1979).

[46] P. G. Harper, *Proc. Phys. Soc. London, Sect. A* **68**, 874 (1955).

[47] S. Aubry and G. André, *Phys. Soc.* **3**, 133 (1980).

[48] D. J. Thouless, *Phys. Rev. B* **28**, 4272 (1983).

[49] G. Roati, C. D'Errico, L. Fallani, M. Fattori, C. Fort, M. Zaccanti, G. Modugno, M. Modugno, and M. Inguscio, *Nature* **453**, 895 (2008).

[50] H. P. Lüschen, S. Scherg, T. Kohlert, M. Schreiber, P. Bordia, X. Li, S. Das Sarma, and I. Bloch, *Phys. Rev. Lett.* **120**, 160404 (2018).

[51] Y. Lahini, R. Pugatch, F. Pozzi, M. Sorel, R. Morandotti, N. Davidson, and Y. Silberberg, *Phys. Rev. Lett.* **103**, 013901 (2009).

[52] Y. E. Kraus and O. Zilberberg, *Phys. Rev. Lett.* **109**, 116404 (2012).

[53] S. Iyer, V. Oganesyan, G. Refael, and D. A. Huse, *Phys. Rev. B* **87**, 134202 (2013).

[54] M. Verbin, O. Zilberberg, Y. E. Kraus, Y. Lahini, and Y. Silberberg, *Phys. Rev. Lett.* **110**, 076403 (2013).

[55] K. A. Madsen, E. J. Bergholtz, and P. W. Brouwer, *Phys. Rev. B* **88**, 125118 (2013).

[56] L.-J. Lang, X. Cai, and S. Chen, *Phys. Rev. Lett.* **108**, 220401 (2012).

[57] M. Tezuka and N. Kawakami, *Phys. Rev. B* **85**, 140508 (2012).

[58] W. DeGottardi, D. Sen, and S. Vishveshwara, *Phys. Rev. Lett.* **110**, 146404 (2013).

[59] S. Ganeshan, K. Sun, and S. Das Sarma, *Phys. Rev. Lett.* **110**, 180403 (2013).

[60] H. Jiang, L.-J. Lang, C. Yang, S.-L. Zhu, and S. Chen, *Phys. Rev. B* **100**, 054301 (2019).

[61] T. Liu, H. Guo, Y. Pu, and S. Longhi, *Phys. Rev. B* **102**, 024205 (2020).

[62] L.-J. Zhai, S. Yin, and G.-Y. Huang, *Phys. Rev. B* **102**, 064206 (2020).

[63] T. Liu and X. Xia, *Phys. Rev. B* **104**, 134202 (2021).

[64] T. Xiao, D. Xie, Z. Dong, T. Chen, W. Yi, and B. Yan, *Science Bulletin* **66**, 2175 (2021).

[65] S. Nakajima, N. Takei, K. Sakuma, Y. Kuno, P. Marra, and Y. Takahashi, *Nature Physics* **17**, 844 (2021).

[66] Y. Liu, X.-P. Jiang, J. Cao, and S. Chen, *Phys. Rev. B* **101**, 174205 (2020).

[67] C. M. Dai, W. Wang, and X. X. Yi, *Phys. Rev. A* **98**, 013635 (2018).

[68] S. Roy, T. Mishra, B. Tanatar, and S. Basu, *Phys. Rev. Lett.* **126**, 106803 (2021).

[69] Y.-T. Hsu, X. Li, D.-L. Deng, and S. Das Sarma, *Phys. Rev. Lett.* **121**, 245701 (2018).

[70] S. Xu, X. Li, Y.-T. Hsu, B. Swingle, and S. Das Sarma, *Phys. Rev. Research* **1**, 032039 (2019).

[71] X. Li, J. H. Pixley, D.-L. Deng, S. Ganeshan, and S. Das Sarma, *Phys. Rev. B* **93**, 184204 (2016).

[72] I. Chang, K. Ikezawa, and M. Kohmoto, *Phys. Rev. B* **55**, 12971 (1997).

[73] F. Liu, S. Ghosh, and Y. D. Chong, *Phys. Rev. B* **91**, 014108 (2015).

[74] Y. Wang, C. Cheng, X.-J. Liu, and D. Yu, *Phys. Rev. Lett.* **126**, 080602 (2021).

[75] Y. Wang, L. Zhang, S. Niu, D. Yu, and X.-J. Liu, *Phys. Rev. Lett.* **125**, 073204 (2020).

[76] L.-Z. Tang, G.-Q. Zhang, L.-F. Zhang, and D.-W. Zhang, *Phys. Rev. A* **103**, 033325 (2021).

[77] Y. E. Kraus, Y. Lahini, Z. Ringel, M. Verbin, and O. Zilberberg, *Phys. Rev. Lett.* **109**, 106402 (2012).

[78] I. I. Satija and G. G. Naumis, *Phys. Rev. B* **88**, 054204 (2013).

[79] R. El-Ganainy, K. G. Makris, M. Khajavikhan, Z. H. Musslimani, S. Rotter, and D. N. Christodoulides, *Nat. Phys.* **14**, 11 (2018).

[80] Y. Ashida, Z. Gong, and M. Ueda, *Advances in Physics* **69**, 249 (2020).

[81] E. J. Bergholtz, J. C. Budich, and F. K. Kunst, *Rev. Mod. Phys.* **93**, 015005 (2021).

[82] Z. Gong, Y. Ashida, K. Kawabata, K. Takasan, S. Higashikawa, and M. Ueda, *Phys. Rev. X* **8**, 031079 (2018).

[83] T. E. Lee, *Phys. Rev. Lett.* **116**, 133903 (2016).

[84] S. Yao and Z. Wang, *Phys. Rev. Lett.* **121**, 086803 (2018).

[85] F. K. Kunst, E. Edvardsson, J. C. Budich, and E. J. Bergholtz, *Phys. Rev. Lett.* **121**, 026808 (2018).

[86] K. Zhang, Z. Yang, and C. Fang, *Phys. Rev. Lett.* **125**, 126402 (2020).

[87] Z. Yang, K. Zhang, C. Fang, and J. Hu, *Phys. Rev. Lett.* **125**, 226402 (2020).

[88] N. Okuma, K. Kawabata, K. Shiozaki, and M. Sato, *Phys. Rev. Lett.* **124**, 086801 (2020).

[89] N. Hatano and D. R. Nelson, *Phys. Rev. Lett.* **77**, 570 (1996).

[90] N. Hatano and D. R. Nelson, *Phys. Rev. B* **56**, 8651 (1997).

[91] Q.-B. Zeng and Y. Xu, *Phys. Rev. Research* **2**, 033052 (2020).

[92] X. Cai, *Phys. Rev. B* **103**, 014201 (2021).

[93] S. Longhi, *Phys. Rev. B* **100**, 125157 (2019).

[94] L. Zhou and W. Han, *Chin. Phys. B* **30**, 100308 (2021).

[95] S. Longhi, *Phys. Rev. Lett.* **122**, 237601 (2019).

[96] Y. Fu, J. H. Wilson, and J. H. Pixley, *Phys. Rev. B* **104**, L041106 (2021).

[97] S. Longhi, *Phys. Rev. Lett.* **122**, 237601 (2019).

[98] F. Song, S. Yao, and Z. Wang, *Phys. Rev. Lett.* **123**, 246801 (2019).